downstream of the jet (15-deg microphone). The actual relationship between the increased entrainment of the symmetry cases and the better acoustic characteristics deserves further study.

The counter-rotating pairs showed a much higher increase, showing little or no noise reduction in the low-frequency noise and as much as a 10-dB increase of the high-frequency noise downstream of the jet. Surks et al.[5] compares all of the cases in detail and showed that the azimuthal (or rotated) angle had little effect in the general acoustic trends and the generator angle of attack increased the high-frequency noise produced.

Overall Sound Pressure Level

The OASPL was obtained by integrating a sound spectrum over all frequencies, yielding a single measure indicative of the total amount of sound at a given spatial location. Figure 4 shows the total sound pressure level for the six different configurations for 20-deg angle of attack. One can see that the noise directly downstream of the nozzle exit is reduced by at least 2 dB by the vortex generators in all cases. Likewise, the off-axis noise is increased in all cases—sometimes by as much as 6 dB. Again, one can see that the better mixed symmetry cases perform better than the vortex pair cases. The effect of increasing the angle of attack corresponds to an increase in off-axis OASPL. The noise downstream of the nozzle remains relatively unaffected by the generator angle of attack. Similar results were found with the case of the rectangular nozzle,[1] although the increase in off-axis noise was not nearly as large.

IV. Conclusion

In conclusion, the results of this work indicate that the acoustic and entrainment effects of introduced streamwise vortex structures are a strong function of vortex sign. Corotating vortices tended to entrain more fluid (up to 50%) without adding as much noise as their counterrotating counterparts. All introduced vorticity showed improved entrainment. Further, the corotating vortices reduced the low-frequency sound by as much as 3 dB, and increased the high-frequency noise by as much as 8 dB. Since most of the low-frequency noise is propagated downstream of the jet, these generator configurations decreased the OASPL downstream of the jet. Since most of the noise off to the side of the jet is high-frequency noise, the generators tended to increase the OASPL in this direction.

These results are qualitatively similar to the results found previously in a rectangular jet, however, the rectangular jet had a smaller increase in the high-frequency noise. This is most likely a result of the fact that the shear layer of the rectangular jet was substantially larger relative to the introduced vorticity (larger nozzle perimeter with same nozzle pressure ratio), implying that the turbulence generated by the vortex generators (same size) was a smaller portion of the total turbulence.

Acknowledgments

This research was conducted in part under the McDonnell Douglas Independent Research and Development program and in part under Tufts University sponsorship. The authors are grateful to Nat Vignati, Joe Kroutil, Mike Meers, and Mark Carletti for assisting in these experiments and in the preparation of this manuscript.

References

[1]Rogers, C. B., and Parekh, D. E., "Mixing Enhancement by and Noise Reduction of Streamwise Vortices in an Air Jet," *AIAA Journal*, Vol. 32, No. 3, 1994, pp. 464–471.

[2]Krishnappa, G., and Csanady, G. T., "An Experimental Investigation of the Composition of Jet Noise," *Journal of Fluid Mechanics*, Vol. 37, June 1969, pp. 149–159.

[3]Ahuji, K. K., and Brown, W. H., "Shear Flow Control by Mechanical Tabs," AIAA Paper 89-0994, March 1989.

[4]Samimy, M., Reeder, M., and Zaman, K., "Supersonic Jet Mixing Enhancement by Vortex Generators," AIAA Paper 91-2263, June 1991.

[5]Surks, P., Rogers, C. B., and Parekh, D., "The Effect of Streamwise Vorticity on the Mixing and Acoustic Characteristics of an Air Jet," Tufts Univ., TF-92-2, Medford, MA, Aug. 1992.

Van Driest Transformation and Compressible Wall-Bounded Flows

P. G. Huang*
Eloret Institute, Palo Alto, California 94303
and
G. N. Coleman†
NASA Ames Research Center, Moffett Field, California 94035

I. Introduction

EXCELLENT agreement was found by Huang et al.,[1] over a range of experiments, between zero pressure gradient (ZPG) compressible turbulent boundary-layer data and a refinement of the "Van Driest-I" density-weighted transformation.[2] The scheme's success supports Fernholz and Finley's[3] recommendation that the law of the wall for incompressible flows can be applied to the transformed velocity in a compressible flow. Zhang et al.,[4,5] however, have recently used experimental results from an earlier report by Fernholz and Finley,[6] and model calculations, to argue that the incompressible value of the von Kármán constant $\kappa = 0.41$ is observed only in the untransformed profiles—despite Fernholz and Finley's opposite conclusion. Zhang et al. have therefore raised some doubts regarding the transformation.

This Note examines the transformation validity question using results from direct numerical simulations (DNS) of supersonic, isothermal (cold) wall channel flow (Coleman et al.[7]). The DNS solutions include two cases: A) with Reynolds number $Re = 3000$, Mach number $M = 1.5$, and channel centerline-to-wall temperature ratio of $T_c/T_w = 1.38$, and B) with $Re = 4880$, $M = 3$, and $T_c/T_w = 2.47$. Here M is based on bulk velocity and wall sound speed; Re on bulk density, bulk velocity, channel half-width, and wall viscosity.[7] Dimensional analysis of the inner layer shows that the law of the wall can be described in terms of two nondimensional wall parameters,[8,9] $M_\tau = u_\tau/c_w \equiv u_\tau/\sqrt{(\gamma-1)\,c_p T_w}$ and $B_q = q_w/(\rho_w c_p u_\tau T_w)$ (where c_p is the constant-pressure specific heat, γ the specific heat ratio, c_w the sound speed based on the wall temperature, q_w the heat flux to the flow from the wall, and $u_\tau = \sqrt{\tau_w/\rho_w}$ with τ_w and ρ_w the stress and density at the wall). Cases A and B are defined by $(M_\tau, B_q) = (0.08, -0.05)$ and $(0.12, -0.14)$. The two cases are therefore very different, with the former values of M_τ and B_q being equivalent to a boundary layer at $M = 2.8$ on a moderately cooled wall with $T_w/T_{aw} \approx 0.4$ (T_{aw} is the adiabatic wall temperature), and the latter equivalent to a layer at $M = 4.5$ over a strongly cooled wall given by $T_w/T_{aw} \approx 0.15$, both at momentum thickness Re (based on freestream conditions) $Re_\theta \approx 4 \times 10^4$. (The M_τ, B_q dependence on freestream bulk parameters in ZPG compressible flows is discussed in Ref. 10.) The DNS results thus represent a wide parameter range and are ideally suited for our purpose of investigating the generality of the Van Driest transformation.

II. Van Driest Law of the Wall

The Van Driest law of the wall can be derived from inner-layer similarity arguments[8,9] leading to "mixing-length" formulas for

Received Sept. 3, 1993; revision March 7, 1994; accepted for publication March 11, 1994. This paper is declared a work of the U.S. Government and is not subject to copyright protection in the United States.

*Research Scientist; Mailing address: M/S 229-1, NASA Ames Research Center, Moffett Field, CA 94035. Senior Member AIAA.

†Postdoctoral Fellow; currently at University of California at Los Angeles, Mechanical, Aerospace, and Nuclear Engineering Department, Los Angeles, CA 90024.

the mean velocity U and temperature T. In terms of the nondimensional parameters $U^+ = U/u_\tau$, $T^+ = T/T_w$, and $y^+ = \rho_w u_\tau y/\mu_w$, the relevant equations are

$$\frac{dU^+}{dy^+} = \frac{(\rho_w/\rho)^{1/2}}{\kappa y^+}$$
$$\frac{dT^+}{dy^+} = -[B_q + (\gamma-1)U^+ M_\tau^2]\, Pr_t \frac{(\rho_w/\rho)^{1/2}}{\kappa y^+} \tag{1}$$

where ρ is the local mean density, κ the von Kármán constant, and Pr_t the turbulent Prandtl number. Combining and integrating Eqs. (1) with respect to U^+,

$$T^+ = C_w - Pr_t B_q U^+ - Pr_t M_\tau^2 U^{+2}(\gamma-1)/2 \tag{2}$$

The constant C_w in Eq. (2) is not necessarily equal to unity, since Eqs. (1) are not valid in the viscous sublayer and the buffer layer. The standard form of the incompressible logarithmic law can be retained if the "Van Driest transformed velocity" is defined by:

$$U_{VD}^+ = \int_0^{U^+} \left(\frac{\rho}{\rho_w}\right)^{1/2} dU^+ = \frac{1}{\kappa} \ln y^+ + C \tag{3}$$

If one further assumes that the density ratio in Eq. (3) can be replaced by T^+ in Eq. (2) with $C_w = 1$, an analytic solution (the well-known Van Driest-I transformation; note that the "Van Driest-II" transformation concerns the skin friction[11]) of Eq. (3) can be obtained[8,9]:

$$U_{VD}^+ \approx \frac{1}{R}\left\{\arcsin\left[\frac{R(U^+ + H)}{D}\right] - \arcsin\left(\frac{RH}{D}\right)\right\} \tag{4}$$

where $R = M_\tau\sqrt{(\gamma-1)Pr_t/2}$, $H = B_q/[(\gamma-1)M_\tau^2]$ and $D = \sqrt{1+R^2H^2}$. Based on available experimental data,[1,3] the values of κ and C in Eq. (3) are found to be similar to their incompressible counterparts, $\kappa \approx 0.40$–0.41 and $C \approx 5.0$–5.2, even though in principle they are functions of M_τ and B_q.

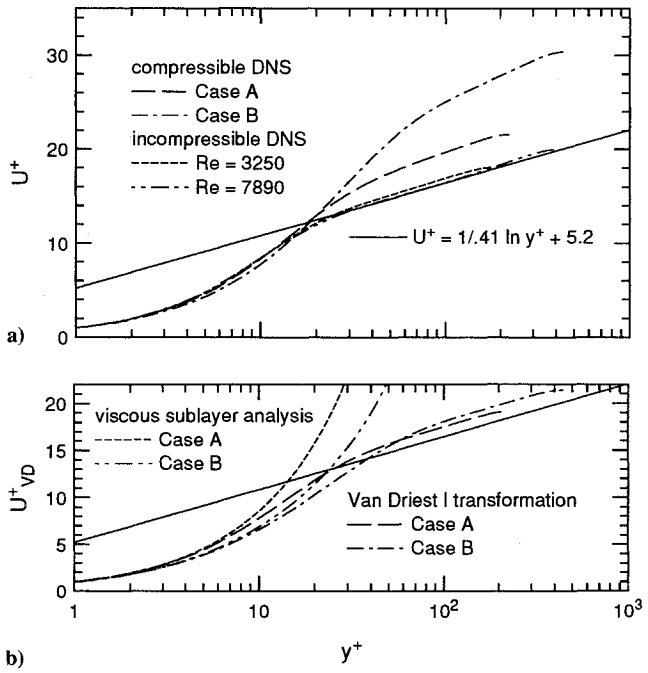

Fig. 1 Comparison of DNS velocity profiles with the log law: a) untransformed and b) transformed velocity.

III. Viscous Sublayer Analysis

In the viscous sublayer (for instance, $y^+ < 5$) where molecular diffusion dominates, the governing equations are

$$\frac{dU_s^+}{dy^+} = \frac{\mu_w}{\mu}$$
$$\frac{dT_s^+}{dy^+} = -[B_q + (\gamma-1)U_s^+ M_\tau^2]\, Pr \frac{\mu_w}{\mu} \tag{5}$$

where μ is the local mean viscosity, Pr is the molecular Prandtl number, and the subscript s indicates "sublayer." Combining and integrating Eqs. (5) with respect to U_s^+,

$$T_s^+ = 1 - PrB_q U_s^+ - PrM_\tau^2 U_s^{+2}(\gamma-1)/2 \tag{6}$$

Applying Eq. (3) to the velocity in the viscous sublayer of Eqs. (5) gives

$$\frac{dU_{VD}^+}{dy^+} = \frac{1}{T^{+0.5}}\frac{\mu_w}{\mu} \approx \frac{1}{T^{+0.5}}\frac{1}{T_s^{+0.7}} \tag{7}$$

where T^+ and T_s^+ are temperature profiles defined by Eqs. (2) and (6), respectively. Since it contains both T^+ and T_s^+, Eq. (7) shows that the Van Driest transformation cannot be used to collapse the sublayer and log-layer velocity profiles simultaneously.

IV. Composite Layer

To describe the profile across the entire layer, we derive a mixing-length model combining the viscous sublayer and the log-law layer. First, the total shear stress at any point is written as the sum of the molecular and Reynolds stresses, $\tau = \tau_w = \mu dU/dy - \rho\overline{uv}$. Second, the Reynolds stress is related to the mean velocity via the mixing-length theory, $-\overline{uv} = l^2 (dU/dy)^2$. After nondimensionalizing, one obtains a quadratic equation for dU^+/dy^+,

$$\frac{dU^+}{dy^+} = \frac{2\mu_w/\mu}{[\sqrt{1 + 4(\mu/\mu_w)^2(\rho/\rho_w)l^{+2}} + 1]} \tag{8}$$

This satisfies two asymptotic conditions: when $y^+ \to 0$, $l^+ = 0$ (in the viscous sublayer), and Eqs. (5) result; when y^+ is sufficiently large, $l^+ = \kappa y^+$ (in the log layer), and Eq. (1) results. To bridge the two regions a "Van Driest damping" is used,[12] with $l^+ = \kappa y^+\{1 - \exp[-y^+(\nu_w/\nu)/A^+]\}$. The value of the damping constant A^+ is chosen to match the incompressible law of the wall; $A^+ = 25.51$. Similarly, by combining molecular and turbulent heat fluxes, the dimensionless temperature equation can be written in terms of $\mu_t = (\rho/\rho_w)l^{+2}\, dU^+/dy^+$ as

$$\frac{dT^+}{dy^+} = -[B_q + (\gamma-1)U^+ M_\tau^2]\frac{Pr_t Pr}{[(\mu_t/\mu_w)Pr + (\mu/\mu_w)Pr_t]} \tag{9}$$

Equations (8) and (9) can be integrated numerically to yield a "complete" law of the wall profile. Assuming appropriate values of κ ($\kappa = 0.41$), γ ($\gamma = 1.4$), and Pr_t ($Pr_t = 0.9$, Ref. 1), the density and viscosity ratios can be related to the temperature ratio T^+ obtained from Eq. (9). Thus, the complete profile depends only on M_τ and B_q.

V. Comparison with DNS

Figure 1a shows the untransformed velocity profiles, U^+ for the DNS results of cases A and B. The profiles do not follow the universal log-law profile, for which we assume $\kappa = 0.41$ and $C = 5.2$. In contrast, the transformed velocity profiles, from Eq. (4), are shown in Fig. 1b. The slopes of the transformed profiles are close

to $1/\kappa = 1/0.41$, the low-speed log-law value, which is also observed in the incompressible channel DNS results[13] in Fig. 1a. The two incompressible cases show that a decrease in Reynolds number does not significantly change κ but is associated with a slight increase of the constant C.

Also shown in Fig. 1b are the viscous sublayer profiles obtained by integrating Eqs. (5) and then applying the transformation of Eq. (4) [or by integrating Eq. (7) directly]. We see that for $y^+ \leq 5$ the sublayer profiles are well represented by the current sublayer analysis. Note that transformed profile differences are larger than untransformed ones in the sublayer region since the transformed velocity is sensitive to the temperature profiles, as in Eq. (7). This difference may be the source of the slight variation of the log-law constant C observed in results of cases A and B. Although it seems plausible that κ is unaltered by moderate compressibility, there is no reason to believe that C will remain equal to the incompressible value as M increases, since C depends on the velocity variation in the sub- and buffer layers.

Velocity and temperature predictions based on the preceding composite mixing-length model are presented in Fig. 2. Comparison with DNS data can be made using either untransformed or transformed velocity profiles. To be consistent with Fig. 1 results, we use the latter; i.e., both the DNS and the model solutions are transformed according to Eq. (4). The velocity and temperature are well represented by the current mixing-length model. (Recall that the current Couette flow analysis is compared with channel flow DNS results; this explains the departure of the predicted temperature from DNS data in the center of the channel, where shear-stress heat generation disappears.) Despite good agreement with the DNS data, since the effects of low Reynolds number on the DNS results cannot be quantified, the present model must be viewed as an engineering guide rather than a rigorous analysis.

To estimate the variation of κ and C found in typical flow conditions, the mixing-length model has been applied to a range of representative M_τ and B_q: $0.02 \leq M_\tau \leq 0.12$ for adiabatic wall conditions ($B_q = 0$) and $-0.02 \leq B_q \leq -0.12$ for $M_\tau = 0.12$. The results—which we feel constitute the key element of the present work—are presented in Fig. 3. The untransformed profiles demonstrate a strong dependence on M_τ and B_q, with κ increasing as M_τ increases and κ decreasing as B_q increases. In contrast, the transformed velocities collapse (in the outer region) near the law-of-the-wall profile, with a nearly constant value of κ and only a slight variation of C. This collapse, when coupled with the similar success for the DNS results presented earlier, supports the usefulness and validity of the Van Driest transformation.

Zhang et al.[4] have recently analyzed $M_\tau = 0.11$ adiabatic-wall boundary-layer data (Fernholz and Finley,[6] case 53011302) and found that the slope of the untransformed log-law plot is close to the incompressible value of κ, whereas the transformed slope is significantly less. The effective Reynolds number,[6] $Re_\theta^* = \rho_e U_e \theta / \mu_w$ (subscript e represents freestream conditions), for this flow is only about 1.3×10^3, however. It is possible that the smaller transformed slope found in both their model prediction and the data could be due to low-Reynolds-number effects that tend to counteract the increase of κ with M_τ observed in Fig. 3b. The effective κ in boundary layers is subject to an Re dependence—decreasing as Re decreases,[14] as the wake region intrudes into the log-layer—that (as the $M = 0$ data in Fig. 1a demonstrates) is not present in channel flow. Therefore, and since conventional turbulence models (for example, those that use rate of turbulent kinetic energy dissipation as a length-scale variable) have been known to underpredict κ for adiabatic wall conditions,[10] the model-data agreement might be restricted to low Re.

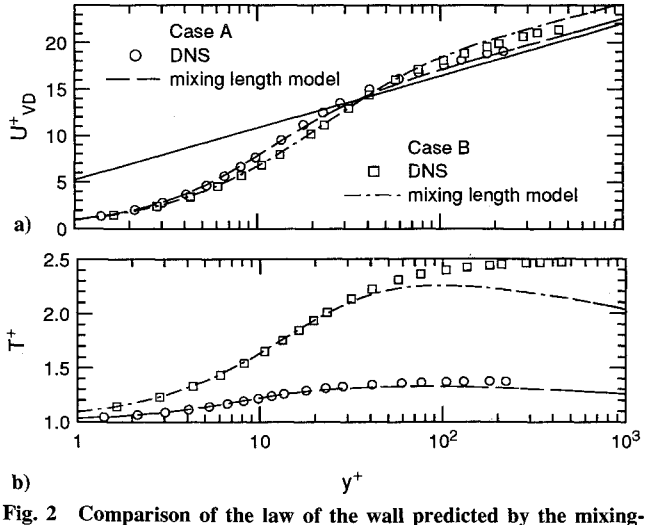

Fig. 2 Comparison of the law of the wall predicted by the mixing-length model, Eqs. (8) and (9), with DNS data: transformed a) velocity and b) temperature.

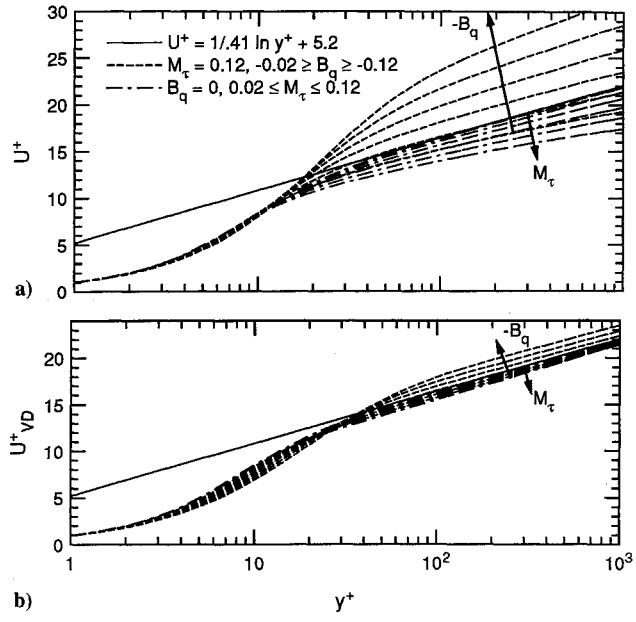

Fig. 3 Variation of velocity profiles for a range of flow conditions: a) untransformed and b) transformed velocity.

Acknowledgment

The authors are grateful to Peter Bradshaw for his comments.

References

[1]Huang, P. G., Bradshaw, P., and Coakley, T. J., "A Skin Friction and Velocity Profile Family for Compressible Turbulent Boundary Layers," *AIAA Journal*, Vol. 31, No. 9, 1993, pp. 1600–1604.

[2]Van Driest, E. R., "Turbulent Boundary Layer in Compressible Fluids," *Journal of Aeronautical Science*, Vol. 18, No. 3, 1951, pp. 145–160.

[3]Fernholz, H. H., and Finley, P. J., "A Critical Commentary on Mean Flow Data for Two-Dimensional Compressible Turbulent Boundary Layers," AGARD-AG-253, May 1980.

[4]Zhang, H. S., So, R. M. C., Speziale, C. G., and Lai, Y. G., "Near-Wall Two-Equation Model for Compressible Turbulent Flows," *AIAA Journal*, Vol. 31, No. 1, 1993, pp. 196–199.

[5]Zhang, H. S., So, R. M. C., Gatski, T. B., and Speziale, C. G., "A Near-Wall Second-Order Closure for Compressible Turbulent Flows," *Near-Wall Turbulent Flows, Proceedings of the International Conference on Near-Wall Turbulent Flows* (Tempe, AZ), Elsevier, Amsterdam, 1993, pp. 209–218.

[6]Fernholz, H. H., and Finley, P. J., "A Critical Compilation of Compressible Turbulent Boundary Layer Data," AGARD-AG-223, June 1977.

[7]Coleman, G. N., Buell, J. C., Kim, J., and Moser, R. D., "Direct Simulation of Compressible Wall-Bounded Turbulence," 9th Turbulent Shear Flows Conference, Kyoto, Japan, Paper 22-2, Aug. 1993.

[8]Rotta, J. C., "Turbulent Boundary Layers with Heat Transfer in Compressible Flow," AGARD Rept. 281, April 1960.

[9]Bradshaw, P., "Compressible Turbulent Shear Layers," *Annual Review of Fluid Mechanics*, Vol. 9, 1977, pp. 33–54.

[10]Huang, P. G., Bradshaw, P., and Coakley, T. J., "Turbulence Models for Compressible Boundary Layers," *AIAA Journal*, Vol. 32, No. 4, 1994, pp. 735–740.

[11]Van Driest, E. R., "The Problem of Aerodynamic Heating," *Aeronautical Engineering Review*, Vol. 15, Oct. 1956, pp. 26–41.
[12]Van Driest, E. R., "On Turbulent Flow Near a Wall," *Journal of Aeronautical Science*, Vol. 23, No. 11, 1956, pp. 1007–1011, 1036.
[13]Kim, J., private communication, NASA Ames Research Center, Moffett Field, CA, June 1993.
[14]Spalart, P. R., "Direct Simulation of a Turbulent Boundary Layer Up To $R_\theta = 1410$," *Journal of Fluid Mechanics*, Vol. 187, Feb. 1988, pp. 61–98.

Assessment of Second-Order Closure Models in Turbulent Shear Flows

Charles G. Speziale*
Boston University, Boston, Massachusetts 02215
and
Thomas B. Gatski†
NASA Langley Research Center, Hampton, Virginia 23681

Introduction

THE need for advanced turbulence models to reliably compute the complex aerodynamic flows of technological interest has led to a resurgence of interest in second-order closure models. Consequently, the recent papers by Shih et al.[1] and Shih and Lumley,[2] which reported tests of second-order closure models in turbulent shear flows, attracted our attention. In these papers, results were presented which appear to indicate that the Shih-Lumley model[3] performs better than two other recently proposed second-order closures in homogeneous shear flow as well as in more complex boundary-free turbulent shear flows. However, our own comparative studies of second-order closure models in benchmark turbulent shear flows have yielded a different picture. The purpose of this Note is to concisely present these alternative results for comparison.

The predictions of three second-order closure models recently proposed by Shih and Lumley,[2,3] Fu et al.,[4] and Speziale et al.[5] will be compared in two benchmark turbulent flows: homogeneous shear flow and the log-layer of an equilibrium turbulent boundary layer. These flows are selected since the former constitutes a basic building-block free turbulent shear flow, whereas the latter serves as a cornerstone for the calculation of practical wall-bounded turbulent flows of engineering interest. Particular attention will be paid to evaluating the ability of each model to accurately predict the equilibrium values for the Reynolds stress anisotropies. Objective means for evaluating the performance of the models are provided, and pitfalls in the formulation and evaluation of models are uncovered that have led to previously published assessments that are misleading.

Turbulent Shear Flows to be Considered

We will consider incompressible turbulent shear flows with the mean velocity gradient tensor

$$\frac{\partial \bar{v}_i}{\partial x_j} = S\delta_{i1}\delta_{j2} \tag{1}$$

where δ_{ij} is the Kronecker delta and S the shear rate. In homogeneous shear flow, the shear rate S is constant and is applied in an unbounded flow domain yielding spatially homogeneous turbulence statistics. For this, as well as any homogeneous turbulence, the Reynolds stress tensor $\tau_{ij} \equiv \overline{u_i u_j}$ is a solution of the transport equation[6]

$$\dot{\tau}_{ij} = -\tau_{ik}\frac{\partial \bar{v}_j}{\partial x_k} - \tau_{jk}\frac{\partial \bar{v}_i}{\partial x_k} + \Phi_{ij} - \varepsilon_{ij} \tag{2}$$

where

$$\Phi_{ij} = \overline{p\left(\frac{\partial u_i}{\partial x_j} + \frac{\partial u_j}{\partial x_i}\right)}, \qquad \varepsilon_{ij} = 2\nu\,\overline{\frac{\partial u_i}{\partial x_k}\frac{\partial u_j}{\partial x_k}} \tag{3}$$

are the pressure-strain correlation and dissipation rate tensor, respectively (here, p is the fluctuating pressure, u_i the fluctuating velocity, ν the kinematic viscosity, and an overbar represents an ensemble mean). One can write

$$\Phi_{ij} - \varepsilon_{ij} = \Pi_{ij} - (2/3)\,\varepsilon\delta_{ij} \tag{4}$$

where $\Pi_{ij} \equiv \Phi_{ij} - {}_D\varepsilon_{ij}$, and ${}_D\varepsilon_{ij}$ is the deviatoric part of the dissipation rate tensor [$\varepsilon \equiv (1/2)\,\varepsilon_{ii}$]. Closure is achieved once models for Π_{ij} and ε are provided. In most existing second-order closure models, Π_{ij} and ε are modeled in the general form

$$\Pi_{ij} = \varepsilon A_{ij}(\boldsymbol{b}) + KM_{ijkl}(\boldsymbol{b})\frac{\partial \bar{v}_k}{\partial x_l} \tag{5}$$

$$\dot{\varepsilon} = -C_{\varepsilon 1}\frac{\varepsilon}{K}\tau_{ij}\frac{\partial \bar{v}_i}{\partial x_j} - C_{\varepsilon 2}\frac{\varepsilon^2}{K} \tag{6}$$

where

$$K = (1/2)\,\tau_{ii}, \qquad b_{ij} = [\tau_{ij} - (2/3)\,K\delta_{ij}]/2K \tag{7}$$

are the turbulent kinetic energy and Reynolds stress anisotropy tensor, respectively. Here, A_{ij} and M_{ijkl} are dimensionless tensor functions of b_{ij} and possibly the turbulence Reynolds number $R_t \equiv K^2/\nu\varepsilon$; $C_{\varepsilon 1}$ and $C_{\varepsilon 2}$ are either constants or functions of the second and third invariants (II, III) of b_{ij} as well as R_t. The full form of the three models to be considered—the Shih-Lumley (SL) model, the Fu, Launder, and Tselepidakis (FLT) model, and the Speziale, Sarkar, and Gatski (SSG) model—are provided in Refs. 2–5.

For homogeneous shear flow, each of the models—consistent with physical and numerical experiments—predicts that the anisotropy tensor b_{ij} and shear parameter SK/ε achieve equilibrium values that are independent of the initial conditions.[7–9] This equilibrium state is associated with solutions where $\dot{b}_{ij} = 0$, or equivalently,

$$\dot{\tau}_{ij} = (\mathcal{P} - \varepsilon)\,\tau_{ij}/K \tag{8}$$

where $\mathcal{P} = -\tau_{ij}\,\partial \bar{v}_i/\partial x_j$ is the turbulence production. The substitution of Eqs. (1) and (8) into Eq. (2) yields the system of algebraic equations[10]

$$-\frac{\tau_{ij}}{K} - \frac{\tau_{12}}{K}\left(\frac{\mathcal{P}/\varepsilon - 1}{\mathcal{P}/\varepsilon}\right) = -\frac{\tau_{i2}}{K}\delta_{j1} - \frac{\tau_{j2}}{K}\delta_{i1} + \Pi^*_{ij} + \frac{2}{3}\frac{\tau_{12}}{K}\left(\frac{\mathcal{P}}{\varepsilon}\right)^{-1}\delta_{ij} \tag{9}$$

where $\Pi^*_{ij} \equiv \Pi_{ij}/SK$ is, for the turbulent shear flows to be considered, a function of τ_{ij}/K and $\mathcal{P}/\varepsilon$ whose specific form depends mainly on the pressure-strain model chosen. In deriving Eq. (9), the identity

$$\frac{\mathcal{P}}{\varepsilon} = -\frac{\tau_{12}}{K}\left(\frac{SK}{\varepsilon}\right) \tag{10}$$

has been used. Once the equilibrium value of $\mathcal{P}/\varepsilon$ is specified [and Eq. (7) is utilized], it is straightforward to obtain the equilibrium values of b_{ij} from a numerical solution of Eq. (9). These equilibrium values are determined almost exclusively by the pressure-strain model.

Received Jan. 31, 1994; revision received May 4, 1994; accepted for publication May 12, 1994.

*Professor, Department of Aerospace and Mechanical Engineering. Member AIAA.
†Senior Research Scientist, Theoretical Flow Physics Branch. Member AIAA.